



## Research article

## Irradiation of UVC LED at 277 nm inactivates coronaviruses in association to photodegradation of spike protein

Qunxiang Ong<sup>a,\*</sup>, J.W. Ronnie Teo<sup>b</sup>, Joshua Dela Cruz<sup>a</sup>, Elijah Wee<sup>a</sup>, Winson Wee<sup>a</sup>, Weiping Han<sup>a,\*\*</sup><sup>a</sup> Institute of Molecular and Cell Biology, Agency for Science, Technology and Research (A\*STAR), 11 Biopolis Way, #02-02, Helios, 138667, Singapore<sup>b</sup> Singapore Institute of Manufacturing Technology (SIMTech), Agency for Science, Technology and Research (A\*STAR), 2 Fusionopolis Way, #08-04, Innovis, 138634, Singapore

## ARTICLE INFO

## Keywords:

UVC disinfection  
Spike protein  
Coronavirus  
277-Nm LED  
Photodegradation

## ABSTRACT

To interrupt SARS-CoV-2 transmission chains, Ultraviolet-C (UVC) irradiation has emerged as a potential disinfection tool to aid in blocking the spread of coronaviruses. While conventional 254-nm UVC mercury lamps have been used for disinfection purposes, other UVC wavelengths have emerged as attractive alternatives but a direct comparison of these tools is lacking with the inherent mechanistic properties unclear. Our results using human coronaviruses, hCoV-229E and hCoV-OC43, have indicated that 277-nm UVC LED is most effective in viral inactivation, followed by 222-nm far UVC and 254-nm UVC mercury lamp. While UVC mercury lamp is more effective in degrading viral genomic content compared to 277-nm UVC LED, the latter results in a pronounced photo-degradation of spike proteins which potentially contributed to the higher efficacy of coronavirus inactivation. Hence, inactivation of coronaviruses by 277-nm UVC LED irradiation constitutes a more promising method for disinfection.

## 1. Introduction

The novel coronavirus SARS-CoV-2 has precipitated into the COVID-19 pandemic, and at the time of writing, resulted in more than millions of infections and deaths. The actual numbers should be much higher than reported, given the high incidence of asymptomatic cases escaping the capture by traditional diagnostic methods. Vaccination, masking, rigorous testing and thorough public disinfection strategies become vital prongs in combating virus spread within communities. Amongst the latter, ultraviolet irradiation presents as an attractive strategy, given its use being well established in inactivating viruses and killing other microbes (Lin et al., 2020; Raeiszadeh and Adeli, 2020). Consequently, UVC mercury lamps have been increasingly deployed in hospital settings.

UVC has been well known to possess germicidal properties and inactivate pathogenic microbes by damaging nucleic acids and proteins, thereby eliminating their ability to reproduce (Rauth, 1965; Sehgal, 1973; Setlow and Carrier, 1966; Werbin et al., 1966). The mechanism at which UV inactivates microbes depends highly on the specific wavelengths. 277nm UVC LEDs (Beck et al., 2017; Kim and Kang, 2018;

Nguyen et al., 2019; Nunayon et al., 2020) and far UVC sources (Welch et al., 2018a, 2018b) have recently emerged as attractive alternatives to UVC mercury lamps. The former does not require mercury, which is banned by the Minamata Convention, has very short turn-on time, and is generally more reliable and has a longer lifetime (Song et al., 2016). The far UVC, on the other hand, is shown to be effective in inactivation of bacteria and human coronaviruses, and potentially poses less safety concerns for deployment (Barnard et al., 2020; Buonanno et al., 2020).

Numerous studies have studied the sensitivity of different microbes to UVC wavelengths, including human coronaviruses (Buonanno et al., 2020; Gerchman et al., 2020) and SARS-CoV-2 (Inagaki et al., 2020; Kitagawa et al., 2020; Storm et al., 2020). However, no study to date has performed a direct comparative study on the efficacy of different UVC wavelengths on inactivation of coronaviruses. In addition, mechanistic insight into how different UVC wavelengths inactivate coronaviruses is severely lacking, and greater understanding in this area would facilitate their deployment in future pandemics. Here, we utilized human coronaviruses, HCoV-229E and OC43, for efficacy studies where 277nm UVC LED consistently outperforms the other UVC wavelengths in inactivating

\* Corresponding author.

\*\* Corresponding author.

E-mail addresses: [ongqx@imcb.a-star.edu.sg](mailto:ongqx@imcb.a-star.edu.sg) (Q. Ong), [wh10@cornell.edu](mailto:wh10@cornell.edu) (W. Han).

coronaviruses. Mechanistic studies suggest that this is achieved via a combination of photo-degradation of spike proteins and RNA molecules.

## 2. Results

### 2.1. Utilizing human coronaviruses for UVC-induced inactivation studies

Coronaviruses are split into the four genera: Alphacoronavirus, Betacoronavirus, Gammacoronavirus and Deltacoronavirus (Fehr and Perlman, 2015; Woo et al., 2010). Among the different genera, alphacoronaviruses and betacoronaviruses have been known to infect mammals, and pose as a significant risk to the human population. The betacoronaviruses, MERS-CoV, SARS-CoV and SARS-CoV-2, may produce severe symptoms in patients while hCoV-OC43 and hCoV-229E cause about 15% of common colds (Figure 1A). In terms of genomic organization, coronaviruses are the largest enveloped RNA viruses with positive single-stranded RNA molecules from 27 to 32 kilobases. The genome comprises of the replicase gene that encodes for the non-structural proteins of the genomes at about 20 kilobases, while similar structural proteins in the form of spike, envelop, membrane and nucleocapsid proteins are interspersed at the 3' end of the genome (Figure 1B).

It has been established that RNA chains are directly disrupted by UVC by formation of pyrimidine dimers (Merriam and Gordon, 1967). The dimerization reaction occurs from adjacent pyrimidine bases in the form of uracil and cytosine (Beukers et al., 2010; Brown and Johns, 1968). We analyzed the genomic content of the coronaviruses based on these sequences as indicated their accession numbers from the NCBI Nucleotide: hCoV-OC43 (MW532119.1), hCoV-229e (KU291448.1) and SARS-CoV-2 (MW403500.1). We found that their overall base composition (Figure 1C) and adjacent base arrangements (Figure 1D) to be similar. We therefore hypothesize that the kinetics of UVC inactivation of hCoV-OC43 and hCoV-229E to be roughly similar.

### 2.2. Inactivation of human coronaviruses after exposure to different UVC wavelengths

To examine the inactivation efficacy of UVC on hCoV-OC43 and hCoV-229E, virus was placed on plastic petri dishes and expose to various UVC wavelengths of  $73 \mu\text{W}/\text{cm}^2$  for different timings ranging from 30 to 300 s (Figures S1–S2). The reduction in infectivity of hCoV-OC43 (Figure 2A, Table S1) and hCoV-229E (Figure 2B, Table S2) can be observed after exposure to different UVC irradiation. The 277-nm UVC LED was most

effective in carrying out the inactivation and achieved 3-log inactivation at  $22 \text{ mJ}/\text{cm}^2$  for both human coronavirus strains, whereas 254-nm UV lamp achieved only 2-log inactivation for hCoV-OC43 and 1-log inactivation for hCoV-229E with the same dosage. Two-way ANOVA analyses of both sets of data reveal significant differences (Table S1-2) between the three UVC wavelengths in carrying out coronavirus inactivation ( $p = 0.0001$  and  $p < 0.0001$  for hCoV-OC43 and hCoV-229E respectively).

We next investigated the integration of hCoV-OC43 in human lung host cells after exposure to 300 s of UVC sources. Figure 2C shows the representative images of human lung cells HCT-8 with hCoV-OC43 illuminated at different UVC wavelengths. We assessed the human cell lines for expression of the viral spike protein and found that 277-nm UVC outperforms the other UVC wavelengths in inactivation of coronaviruses.

### 2.3. Examining rates of nucleotide degradation under different UVC wavelengths

To understand if the inactivation efficacy comes from RNA damage, we performed quantitative RT-PCR to examine the copy number of hCoV-OC43 after UVC irradiation. We observed that the copy number of hCoV-OC43 to be unperturbed after 300 s of 222-nm far UVC irradiation, while 254-nm UV lamp exerted the largest decrease in copy number followed by 277-nm UVC LED (Figure 3A).

### 2.4. Photodegradation of hCoV-OC43 spike protein under 277-nm UVC LED

We next hypothesized that molecular components other than nucleic acids could be implicated, and the spike protein is an especially attractive target to pursue given that it facilitates viral transmission by binding to the host receptors (Shang et al., 2020). To this end, we subjected hCoV-OC43 to different duration of 254-nm and 277-nm UVC irradiation, and observed through Western blot that the spike protein is degraded under 277-nm UVC LED and not under 254-nm UVC lamp. Silver staining of the viral lysate indicates the overall amount of protein loaded in each lane (Figure 3B). To further confirm that spike protein is indeed degraded by 277-nm UVC LED, we performed UVC illumination on purified hCoV-OC43 spike proteins in vitro. Silver staining as depicted in Figure 3C shows that hCoV-OC43 spike protein presents at a lower intensity under 277-nm UVC LED and not under 254-nm UV lamp. This is further corroborated by absorbance spectroscopy in Figure 3C which demonstrates a shift in absorbance upon 277-nm UVC LED illumination but not 254-nm UV lamp.

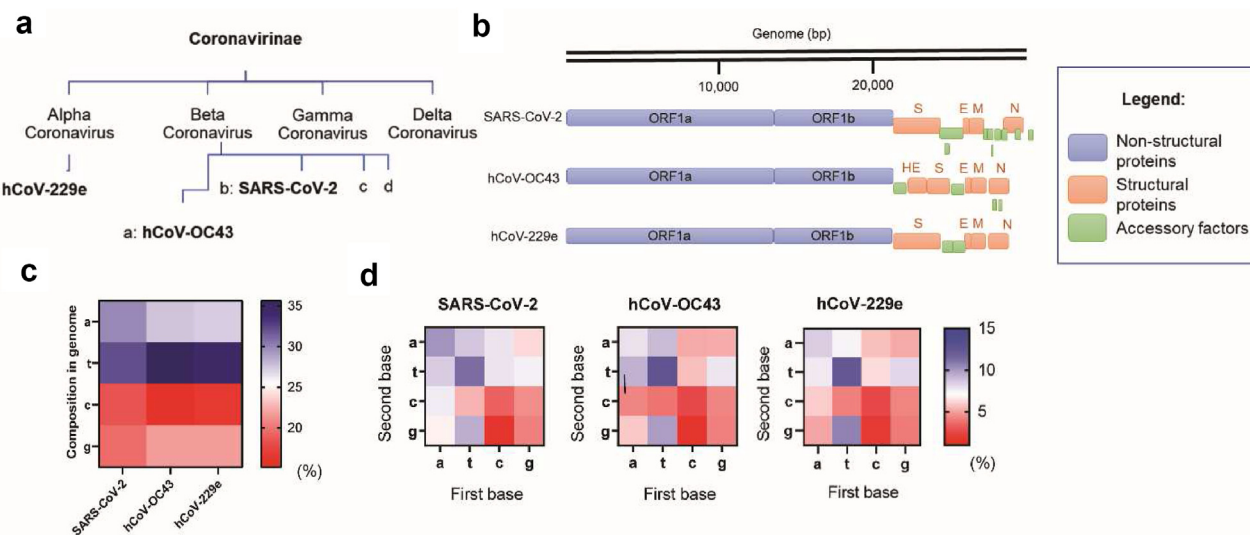


**Figure 1.** Utilizing human coronaviruses for UVC-induced inactivation studies (a) The different genera of the coronavirus family. Alpha and beta-coronaviruses with the various highlighted viruses, hCoV-229e, hCoV-OC43 and SARS-CoV-2. (b) Genome organizations of SARS-CoV-2, hCoV-OC43 and hCoV-229e. (c) Overall base composition of SARS-CoV-2, hCoV-OC43 and hCoV-229e. (d) Adjacent base composition of SARS-CoV-2, hCoV-OC43 and hCoV-229e.

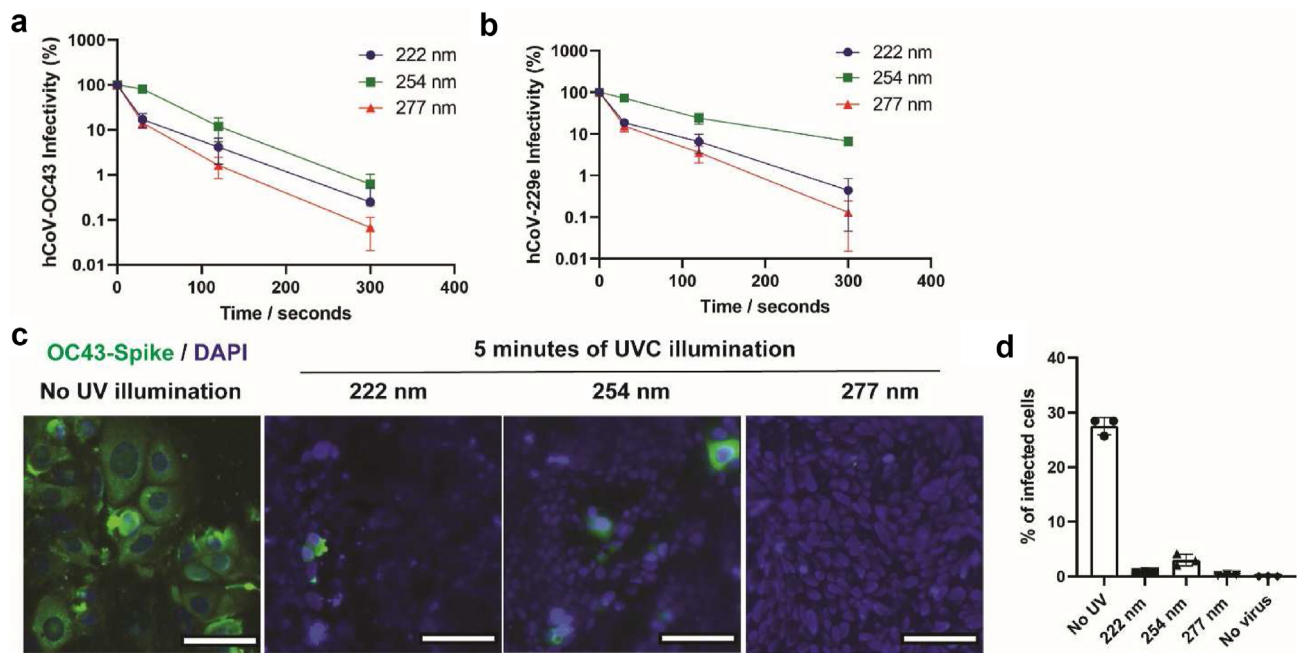


**Figure 2.** Inactivation of human coronaviruses after exposure to different UVC wavelengths (a) hCoV-OC43 infectivity as a function of the duration of different UVC sources at  $73 \mu\text{W}/\text{cm}^2$ . Infectivity is defined as a function of  $\text{PFU}_{\text{UV}}/\text{PFU}_{\text{NoUV}}$ . Values are reported as mean  $\pm$  SD from  $n = 3$  experiments. (b) hCoV-229e infectivity as a function of the duration of different UVC sources at  $73 \mu\text{W}/\text{cm}^2$ . Infectivity is defined as a function of  $\text{PFU}_{\text{UV}}/\text{PFU}_{\text{NoUV}}$ . Values are reported as mean  $\pm$  SD from  $n = 3$  experiments. (c) Infection of human lung cell line, HCT-8 from irradiated and untreated hCoV-OC43. Green fluorescence indicates infected cells while blue fluorescence indicates DAPI stains of nuclei. Images were acquired with a 40x objective, with the scale bars at  $50 \mu\text{m}$ . (d) Quantification of HCT-8 cells infected with irradiated and untreated hCoV-OC43. Values are reported as mean  $\pm$  SD from  $n = 3$  experiments.

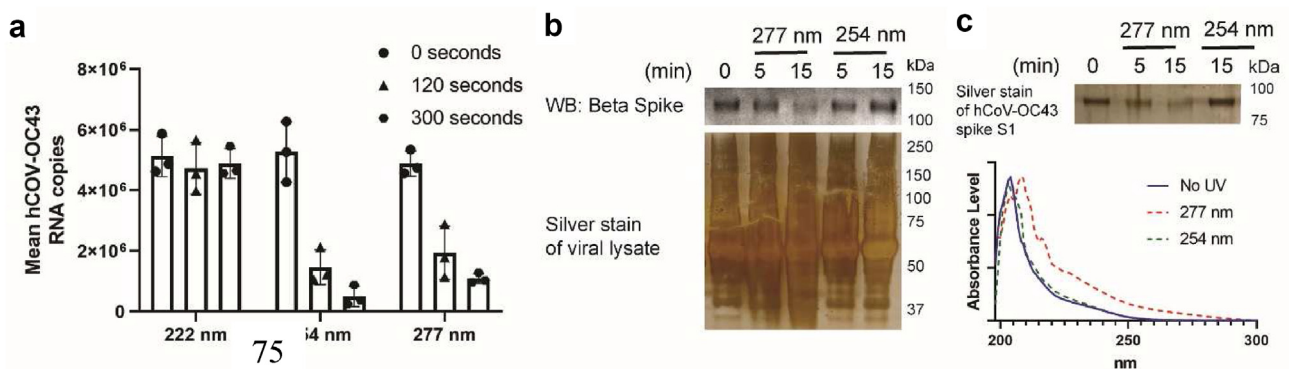


**Figure 3.** 277nm UVC LED's higher efficacy at inactivation of coronavirus is not due to UV-induced genomic damage and could be due to spike protein degradation. (a) Quantitative RT-PCR reveals that the copy number of hCoV-OC43 did not change due to 222-nm illumination, and decrease the fastest due to 254-nm UVC lamp. Values are reported as mean  $\pm$  SD from  $n = 3$  experiments. (b) Beta spike glycoprotein of hCoV-OC43 is found to diminish in intensity upon 15 min of 277-nm UVC LED illumination but not under 254-nm UVC lamp. Silver stain of viral lysate is provided to show the total loading on each lane. Full uncropped figures are available at Figure S3. (c) Purified hCoV-OC43 spike S1 proteins is found to diminish in intensity upon 15 min of 277-nm UVC LED illumination but not under 254-nm UVC lamp. Changes in absorbance spectra of hCoV-OC43 spike S1 observed after 15 min of 277-nm UVC LED irradiation but not 254-nm UVC lamp. Full uncropped figure is available at Figure S3.

### 2.5. Photodegradation of SARS-CoV-2 spike protein under 277-nm UVC LED

First, we exposed SARS-CoV-2 spike protein S1 subunit to varied durations of 254-nm UVC lamp and 277-nm UVC LED and observed the reduction of the full-length spike protein band under 277-nm UVC LED and not under 254-nm UVC LED. This happens on both glycosylated and non-glycosylated forms of the spike protein (Figure 4A). Absorbance spectroscopy (Figure 4B) analysis showed the UV absorbance profile of 254-nm lit proteins to be relatively unchanged while there is an increase of absorbance profile in the 250–300 nm region for 277-nm lit proteins. Western blot (Figure 4C) analysis further revealed a reduction in the SARS-CoV-2 spike S1 proteins under low loading of protein samples, but

under higher loadings, aggregates of spike protein in the form of dimers and trimers could be seen in a dose-dependent manner.

In the search for potential mechanisms that drive the absorption of 277-nm wavelengths and degradation/aggregation of the proteins, we studied the structure of the SARS-CoV-2 S glycoprotein (PDB: 6VXX) (Walls et al., 2020) and looked for aromatic amino acids in proximity to disulfide bonds as possible active regions upon 277-nm UVC irradiation. In particular, tryptophan has high molar absorptivity at the 280-nm wavelength and has been known to mediate energy transfer and neighboring disulfide bond breakage (Beaven and Holiday, 1952; Chan et al., 2006; Kerwin and Remmele, 2007; Wu et al., 2008). We identified the Trp 436 as a key antenna of 277-nm absorption, and conducted studies on W436R receptor binding domain (RBD) mutant alongside wild type, F377L and Y453F

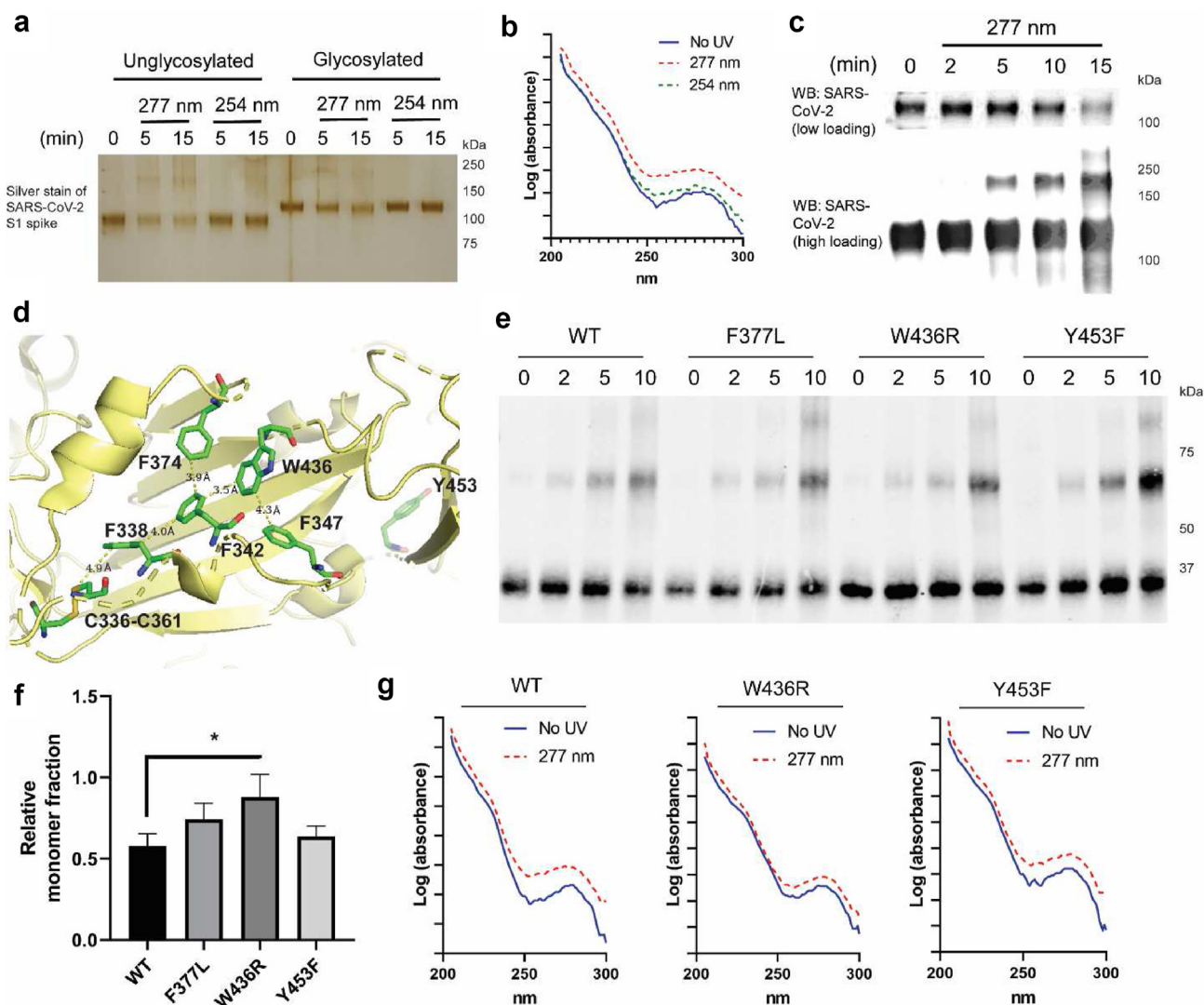


**Figure 4.** Photodegradation of SARS-CoV-2 spike protein under 277nm UVC LED (a) Silver stains of un-glycosylated and glycosylated SARS-CoV-2 spike S1 protein under different UVC treatment. Full uncropped figure is available at Figure S3. (b) Changes in absorbance spectra of SARS-CoV-2 spike S1 observed after 15 min of 277-nm UVC LED irradiation but not 254-nm UVC lamp. (c) Western blot analysis of SARS-CoV-2 spike S1 protein revealed that while the protein level of SARS-CoV-2 decreases under 277-nm UVC LED, higher aggregates could be observed upon higher UVC dose. Full uncropped figure is available at Figure S3. (d) SARS-CoV2 spike protein structure (PDB: 6VXX). Key residues centered around W436 that could potentially act as an antenna for 277nm UVC absorption. Y453 is depicted in the background while F377 is adjacent to F374 (not highlighted in the schematic). (e) Western blot analysis of SARS-CoV-2 spike S1 RBD proteins revealed the differential rate of aggregation and degradation amongst the different mutants. Full uncropped figure is available at Figure S3. (f) Quantification of relative monomer fraction for wild type and mutant RBD proteins. The fraction is calculated as a function of (intensity at 35kDa)/(overall intensity across the whole lane). (g) Absorbance spectra of the RBD proteins reveal little changes in 250–300 nm UVC absorbance for W436R compared to wild type and Y453F mutant, indicating potentially that W436R spike protein is less susceptible to 277nm UVC LED treatment.

mutants, that are in close proximity but unlinked to the W436–C336–C361 transfer chain (Figure 4D). We illuminated the RBD samples with 0, 2, 5, 10 min of 277-nm UVC LED and studied the rate of oligomerization for each sample by probing with SARS-CoV-2 Spike antibody (Figure 4E). It is observed that W436R mutant has a lower rate of aggregation compared to the other species and this is quantified by comparing the intensity of the monomer fraction (at 35kDa) with respect to the rest of the lane for samples illuminated with 5 min of 277-nm UVC LED (Figure 4F). Absorbance spectroscopy further verified that after 10 min of UVC LED illumination, the W436R mutant did not exhibit as significant changes in absorbance compared to the wild-type and Y453F mutant.

### 3. Discussion

In this study, we focused on human coronaviruses hCoV-OC43 and hCoV-229E, which belong to the genus beta-coronavirus and alpha-

coronavirus respectively. In particular, hCoV-OC43 could be considered as a surrogate for SARS-CoV-2 and the conclusions drawn here on UVC efficacy can thus be extrapolated to SARS-CoV-2. On the other hand, hCoV-229E resembles the viruses that causes the common cold. The viral efficacy tests performed here not only targeted the current COVID-19 pandemic, but also applies to future coronaviral pandemics in general.

While many studies have individually tested the 222-nm far UVC lamp, 254-nm UVC lamp and broad ranges of UVC LEDs for their efficacy towards viruses, this is the first study to report the mechanisms through which viral inactivation occurs. In summary, we find that 277-nm UVC LED outperforms the other UVC wavelengths in inactivation of human coronaviruses, and this could be aided by the contribution from spike protein degradation with absorption of UV wavelengths at Trp 436. We also find that 222-nm UVC LED does not affect the genomic material of beta-coronavirus, an observation that is congruent with a previous report (Kitagawa et al., 2020).

It has been widely believed that the efficacy of UV germicidal irradiation (UVGI) is dependent largely on the absorption by the target nucleic acids. While the mechanism holds significant merit, it is important to examine the other molecular mechanisms at which UV tools could exert their germicidal properties. It is thus important to consider the viral components individually as we characterize the multitude of UVGI solutions available to combat the current and future pandemics.

#### 4. Limitations of study

Due to the lack of access to BSL-3 facilities, we are unable to perform the viral infectivity tests on SARS-CoV-2 or the relevant variants. However, this limitation is mitigated by our studies on the beta coronavirus hCoV-OC43, which provides a close approximation towards SARS-CoV-2 with the relevant structures of the spike proteins being relatively similar.

#### Declarations

##### Author contribution statement

Qunxiang Ong, Ph. D: Conceived and designed the research; Performed the experiments; Analyzed and interpreted the data; Contributed reagents, materials, analysis tools or data; Wrote the paper.

J.W. Ronnie Teo: Conceived and designed the research; Performed the experiments; Analyzed and interpreted the data; Contributed reagents, materials, analysis tools or data.

Joshua Dela Cruz and Winson Wee: Performed the experiments; Analyzed and interpreted the data.

Elijah Wee: Performed the experiments.

Weiping Han: Conceived and designed the research; Wrote the paper.

##### Funding statement

Dr Qunxiang Ong was supported by National Research Foundation Singapore [NRF2020NRF-CG002-035].

J.W. Ronnie Teo was supported by Accelerate Technologies [GAP/2020/00392].

##### Data availability statement

Data will be made available on request.

##### Declaration of interests statement

The authors declare no conflict of interest.

##### Additional information

Supplementary content related to this article has been published online at <https://doi.org/10.1016/j.heliyon.2022.e11132>.

##### Acknowledgements

We thank Dr. Edward George Robins, Dr. Yaw-Sing Tan, Dr. Janarthanan Krishnamoorthy and Ms. Haitong Mao for proofreading of the manuscript; we thank Prof. Lisa Ng, Prof. Xianjun Loh, Dr. Yuanjie Liu, Ms. Siew Lan Lim and Dr. Sun-Yee Kim for providing technical advice and help.

## Materials and Methods

### Key Resources Table

REAGENT or RESOURCE	SOURCE	IDENTIFIER
<b>Antibodies</b>		
Anti-Coronavirus OC43 Spike Protein antibody	Cusabio	CSB-PA336163EA01HIY
SARS-CoV-2 Spike RBD antibody	Sinobiological	40592-T62
<b>Bacterial and virus strains</b>		
HCoV-229E	ATCC	VR-740
HCoV-OC43	ATCC	VR-1588
<b>Chemicals, peptides, and recombinant proteins</b>		
EMEM	ATCC	30–2003
RPMI-1640	ATCC	30–2011
Purified recombinant spike proteins	Sinobiological	40592-V08H80, 40591-V08H3, 40592-V08H9, 40592-V08H27, 40591-V08H, 40607-V08H1
Carboxymethylcellulose	Sigma Aldrich	C4888
<b>Critical commercial assays</b>		
QiAmp Viral RNA mini kit	Qiagen	
TaqPath 1-step RT-qPCR master mix CG	Applied Biosystems	
Pierce™ Silver Stain Kit	ThermoFisher	
<b>Deposited data</b>		
SARS-CoV-2 Spike Protein	PDB	6VXX
hCoV-OC43	NCBI Nucleotide database	MW532119.1
hCoV-229e	NCBI Nucleotide database	KU291448.1
SARS-CoV-2	NCBI Nucleotide database	MW403500.1

(continued on next page)

(continued)

REAGENT or RESOURCE	SOURCE	IDENTIFIER
Experimental models: Cell lines		
MRC-5	ATCC	CCL-171
HCT-8	ATCC	CCL-244
Oligonucleotides		
Forward Primer for qRT-PCR of hCoV-OC43: 5'-ATGTTAGGCCGATAATTGAGGACTAT-3'	Vjigen et al.	
Reverse Primer for qRT-PCR of hCoV-OC43: 5'-AATGTAAGATGGCCGCGTATT-3'	Vjigen et al.	
Software and algorithms		
ImageJ	Schneider et al., 2012	<a href="https://imagej.nih.gov/ij/">https://imagej.nih.gov/ij/</a>
GraphPad Prism Software 8.4.3	GraphPad Inc.	
Quantstudio 5 software	Applied Biosystems	
Other		
222-nm far UVC lamp	Ushio	N.A.
254-nm UVC mercury lamp	Sankyo Denki	G8T5
277-nm UVC LED	Lextar	PU35CM1
Spectroradiometer	GL Optic	GL Spectis 4.0

### Viral strains and viral propagation

hCoV-229E (ATCC VR-740) and hCoV-OC43 (ATCC VR-1558) were propagated in human lung fibroblasts MRC-5 (ATCC CCL-171) and colon adenocarcinoma cells HCT-8 (ATCC CCL-244) respectively (all from ATCC, Manassas, VA). The MRC-5 fibroblasts were grown in EMEM (ATCC 30–2003) supplemented with 10% Fetal Bovine Serum (FBS), 100 U/ml penicillin and 100 µg/ml streptomycin (Sigma-Aldrich, St. Louis, MO). The HCT-8 epithelial cells were cultured in RPMI-1640 supplemented with 10% horse serum, 100 U/ml penicillin and 100 µg/ml streptomycin. The virus infection medium is made up of EMEM or RPMI-1640 with 2% FBS or horse serum for hCoV-229E and hCoV-OC43 respectively.

### UV sources and irradiance measurement

To understand the effect of UVC wavelength on human coronaviruses, three different UVC light sources – 222-nm far UVC lamp (Ushio), 254-nm UVC mercury lamp (Sankyo Denki G8T5) and 277-nm UVC LED (Lextar PU35CM1) were used in this study. These UVC light sources were measured using a calibrated spectroradiometer (GL Spectis 4.0) with an absolute measurement uncertainty of less than 6%. To provide a comparative UVGI efficacy study between these UVC light sources, the radiant intensity of the far UVC and mercury lamp is measured at different distances while the UVC LEDs are driven at different constant drive currents to obtain a common UV intensity of 73 µW/cm<sup>2</sup>. The UVC LED, with a beam angle of 120°, is assembled into a 5 × 5 array at a working distance of 12 cm to ensure uniform UV intensity across the surface of the Petri dish. The relative wavelength spectra of the light sources are shown in Figure S1. Based on the UV intensity readings, an enclosure is fabricated for each light source and the radiant intensity of the enclosure is further validated with the spectroradiometer as shown in Figure S2.

### Viral infectivity experiments

The virus was propagated as previously described and stored in virus infection medium at 10<sup>8</sup> PFU/ml. In one sitting, we have cultured 10 plates of MRC-5 or HCT-8 cells at 10 million cells per T175 flask, and the viruses hCoV-229e or hCoV-OC43 are propagated for 60 h and clarified by centrifugation. The initial PFU was then derived via the following experimental steps. MRC-5 cells or HCT-8 cells were seeded in 12-well plates and incubated at 37 °C, 5 % CO<sub>2</sub> until 80–90 % confluent. Cells were inoculated with serial 10-fold dilutions of each virus sample in triplicate. The inoculum was adsorbed for 1 h at 37 °C, 5 % CO<sub>2</sub> with periodic shaking every 10 min. The inoculum was then removed and 1 % methylcellulose (Millipore Sigma) in DMEM with 2% heat-inactivated FBS was added. The plates were incubated at 37 °C, 5 % CO<sub>2</sub> for 3 days. Fixation with 4% paraformaldehyde was performed at room temperature for an hour. Staining with 0.5% crystal violet was then conducted and the plaques are then quantified. Plates were air-dried, plaques enumerated and titre calculated. For each irradiation, 100 µl of virus suspension was placed on a 3-cm Petri dish. After each irradiation, the virus was subjected to serial dilution of 5 times, and 50 µl of each condition is diluted with 450 µl of virus infection medium into 24-hour old and 80–90 % confluent MRC-5 or HCT-8 cells in 6-well plates. The cells were incubated with the virus for 1 h in a humidified incubator with 5% CO<sub>2</sub> before addition of a liquid overlay medium, 3% carboxymethylcellulose, is applied to the cells to restrict virus growth to the originally infected loci of cells. The cells are incubated at 37C in a 5% CO<sub>2</sub> incubator for 3 days before the liquid overlay medium is aspirated and fixation with 4% paraformaldehyde is performed at room temperature for an hour. Staining with 0.5% crystal violet is then conducted and the plaques are then quantified.

### Immunofluorescence experiments

To assess whether 5 min of various UVC illumination reduces the number of infected cells, immunostaining was performed to detect the presence of OC43 viral particles in the host human cells. Briefly, 2 × 10<sup>5</sup> HCT-8 cells were plated in each Petri dish one day before the experiment. The viral suspension after their respective treatments was overlaid on the monolayer of host cells. After 1 h of incubation, the cells were washed with PBS and incubated for two days in fresh medium. The cells were then fixed with 4% paraformaldehyde at room temperature for 15 min and washed with PBS before being labelled with anti-Coronavirus OC43 Spike Protein antibody (CusaBio Technology LLC, Houston, TX, USA) 1:500 in PBS containing 2 %

bovine serum albumin (BSA) and 0.1 % TBS-T. Cells were then washed with PBS and labelled with goat anti-rabbit Alexa Fluor-488 (Life Technologies, Grand Island, NY) in PBS containing 2 % BSA at room temperature for an hour with gentle shaking. Following washing with PBS, the cells were stained with DAPI and observed with the 40x objective of Nikon Ti-2 TIRF microscope.

### Reverse Transcriptase Experiments

Beta-coronavirus RNA was extracted from the viral samples on each Petri dish using the QiAmp Viral RNA mini kit (Qiagen) following the manufacturer's instructions. 5 µl of each sample was used for qRT-PCR analysis utilizing the TaqPath 1-step RT-qPCR master mix CG (Applied Biosystems) and the primer set spanning a target region of 68bp for HCoV-OC43 as reported (Vijgen et al., 2005). The forward primer is 5'-ATGTTAGGCCGA-TAATTGAGGACTAT-3 and the reverse primer is 5'-AATGTAAGATGGCCGCGTATT-3'. The analysis was then performed using the Quantstudio 5 software.

### Protein degradation experiments

The antibodies that were utilized for western blots in this paper includes anti-Coronavirus OC43 Spike Protein antibody (CusaBio Technology LLC, Houston, TX, USA) and SARS-CoV-2 Spike RBD antibody (SinoBiological). All coronavirus purified spike proteins were obtained from SinoBiological. All samples for Western blot were lysed in 2x Lamelli buffer and incubated in room temperature for 20 min before loading. Approximately 200 ng of protein sample is loaded for silver staining experiments and 1µg of protein sample is loaded for Western blot experiments. The lysates were then subjected to SDS gel electrophoresis. For silver staining, we utilized the Pierce™ Silver Stain Kit (ThermoFisher). For Western blot, the samples were transferred to nitrocellulose membranes using iBlot2 (Life Technologies), blocked with 5% BSA in TBST and incubated with primary antibodies in 5% BSA. Membranes were then incubated with rabbit-IRDye 800 CW secondary antibodies and imaged on an Odyssey CLx (LI-COR). Absorption spectroscopy was performed on Nanodrop (ThermoFisher).

### Quantification and Statistical Analyses

The number of replicates (n) are indicated in the respective figure legends. For all statistical tests, significance was measured against  $p < 0.05$ . For comparisons of infectivity curves, 2-way analyses of variance (ANOVA) were carried out with the different UVC wavelengths and exposure time as the factors. All statistical analyses were performed with the GraphPad Prism Software 8.4.3 (GraphPad Software Inc., La Jolla, CA, USA) and all values are expressed as means  $\pm$  standard deviation.

### Protein structure studies

The Desktop PyMOL 2.4 was used to visualize the protein structure of SARS-CoV-2 S glycoprotein (Protein Data Bank 6VXX) and calculate the distances between each indicated residue.

## References

- Barnard, I.R.M., Eadie, E., Wood, K., 2020. Further evidence that far-UVC for disinfection is unlikely to cause erythema or pre-mutagenic DNA lesions in skin. *Photodermatol. Photoimmunol. Photomed.* 36, 476–477.
- Beaven, G.H., Holiday, E.R., 1952. Ultraviolet absorption spectra of proteins and amino acids. *Adv. Protein Chem.* 7, 319–386.
- Beck, S.E., Ryu, H., Boczek, L.A., Cashdollar, J.L., Jeanis, K.M., Rosenblum, J.S., Lawal, O.R., Linden, K.G., 2017. Evaluating UV-C LED disinfection performance and investigating potential dual-wavelength synergy. *Water Res.* 109, 207–216.
- Beukers, R., Ylstra, J., Berends, W., 2010. The effect of ultraviolet light on some components of the nucleic acids: II: in rapidly frozen solutions. *Recl. Des Trav. Chim. Des Pays-Bas* 77, 729–732.
- Brown, I.H., Johns, H.E., 1968. Photochemistry of uracil. intersystem crossing and dimerization in aqueous solution. *Photochem. Photobiol.* 8, 273–286.
- Buonanno, M., Welch, D., Shuryak, I., Brenner, D.J., 2020. Far-UVC light (222 nm) efficiently and safely inactivates airborne human coronaviruses. *Sci. Rep.* 10, 1–8.
- Chan, H.-L., Gaffney, P.R., Waterfield, M.D., Anderle, H., Peter Matthiessen, H., Schwarz, H.-P., Turecek, P.L., Timms, J.F., 2006. Proteomic analysis of UVC irradiation-induced damage of plasma proteins: serum amyloid P component as a major target of photolysis. *FEBS Lett.* 580, 3229–3236.
- Fehr, A.R., Perlman, S., 2015. Coronaviruses: an overview of their replication and pathogenesis. In: *Coronaviruses: Methods and Protocols*. Springer, New York, pp. 1–23.
- Gerchman, Y., Mamane, H., Friedman, N., Mandelboim, M., 2020. UV-LED disinfection of Coronavirus: wavelength effect. *J. Photochem. Photobiol. B Biol.* 212, 112044.
- Inagaki, H., Saito, A., Sugiyama, H., Okabayashi, T., Fujimoto, S., 2020. Rapid inactivation of SARS-CoV-2 with deep-UV LED irradiation. *Emerg. Microb. Infect.* 9, 1744–1747.
- Kerwin, B.A., Remmele, R.L., 2007. Protect from light: Photodegradation and protein biologics. *J. Pharmacol. Sci.* 96, 1468–1479.
- Kim, D.K., Kang, D.H., 2018. UVC LED irradiation effectively inactivates aerosolized viruses, bacteria, and fungi in a chamber-type air disinfection system. *Appl. Environ. Microbiol.* 84.
- Kitagawa, H., Nomura, T., Nazmul, T., Omori, K., Shigemoto, N., Sakaguchi, T., Ohge, H., 2020. Effectiveness of 222-nm ultraviolet light on disinfecting SARS-CoV-2 surface contamination. *Am. J. Infect. Control* 49, 299–301.
- Lin, Q., Lim, J.Y.C., Xue, K., Yew, P.Y.M., Ow, C., Chee, P.L., Loh, X.J., 2020. Sanitizing agents for virus inactivation and disinfection. *View*, 1.
- Merriam, V., Gordon, M.P., 1967. Pyrimidine dimer formation in ultraviolet irradiated TMV-RNS. *Photochem. Photobiol.* 6, 309–319.
- Nguyen, T.M.H., Suwan, P., Koottatep, T., Beck, S.E., 2019. Application of a novel, continuous-feeding ultraviolet light emitting diode (UV-LED) system to disinfect domestic wastewater for discharge or agricultural reuse. *Water Res.* 153, 53–62.
- Nunayon, S.S., Zhang, H., Lai, A.C.K., 2020. Comparison of disinfection performance of UVC-LED and conventional upper-room UVGI systems. *Indoor Air* 30, 180–191.
- Raeiszadeh, M., Adeli, B., 2020. A critical review on ultraviolet disinfection systems against COVID-19 outbreak: applicability, validation, and safety considerations. *ACS Photonics* 7, 2941–2951.
- Rauth, A.M., 1965. The physical state of viral nucleic acid and the sensitivity of viruses to ultraviolet light. *Biophys. J.* 5, 257–273.
- Schneider, C., Rasband, W., Eliceiri, K., 2012. NIH Image to ImageJ: 25 years of image analysis. *Nat. Methods* 9, 671–675.
- Sehgal, O.P., 1973. Inactivation of southern bean mosaic virus and its ribonucleic acid by nitrous acid and ultraviolet light. *J. Gen. Virol.* 18, 1–10.
- Setlow, R.B., Carrier, W.L., 1966. Pyrimidine dimers in ultraviolet-irradiated DNA's. *J. Mol. Biol.* 17, 237–254.
- Shang, J., Wan, Y., Luo, C., Ye, G., Geng, Q., Auerbach, A., Li, F., 2020. Cell entry mechanisms of SARS-CoV-2. *Proc. Natl. Acad. Sci. U.S.A.* 117, 11727–11734.
- Song, K., Mohseni, M., Taghipour, F., 2016. Application of ultraviolet light-emitting diodes (UV-LEDs) for water disinfection: a review. *Water Res.* 94, 341–349.
- Storm, N., McKay, L.G.A., Downs, S.N., Johnson, R.I., Birru, D., de Samber, M., Willaert, W., Cennini, G., Griffiths, A., 2020. Rapid and complete inactivation of SARS-CoV-2 by ultraviolet-C irradiation. *Sci. Rep.* 10, 1–5.
- Vijgen, L., Keyaerts, E., Moës, E., Maes, P., Duson, G., Van Ranst, M., 2005. Development of one-step, real-time, quantitative reverse transcriptase PCR assays for absolute quantitation of human coronaviruses OC43 and 229E. *J. Clin. Microbiol.* 43, 5452–5456.
- Walls, A.C., Park, Y.J., Tortorici, M.A., Wall, A., McGuire, A.T., Veesler, D., 2020. Structure, function, and antigenicity of the SARS-CoV-2 spike glycoprotein. *Cell* 181, 281–292.e6.
- Welch, D., Buonanno, M., Grilj, V., Shuryak, I., Crickmore, C., Bigelow, A.W., Randers-Pehrson, G., Johnson, G.W., Brenner, D.J., 2018a. Far-UVC light: a new tool to control the spread of airborne-mediated microbial diseases. *Sci. Rep.* 8, 2752.
- Welch, D., Spotnitz, H.M., Brenner, D.J., Randers-Pehrson, G., Buonanno, M., Shuryak, I., 2018b. Far-UVC light applications: sterilization of MRSA on a surface and

- inactivation of aerosolized influenza virus. In: Dai, T. (Ed.), *Light-Based Diagnosis and Treatment of Infectious Diseases*. SPIE, p. 60.
- Werbin, H., Hidalgo-Salvatierra, O., Seear, J., McLaren, A.D., 1966. Comparative photoreactivation of ultraviolet light-inactivated tobacco mosaic virus ribonucleic acid on *Chenopodium*, pinto bean, and tobacco plants. *Virology* 28, 202–207.
- Woo, P.C.Y., Huang, Y., Lau, S.K.P., Yuen, K.-Y., 2010. Coronavirus genomics and bioinformatics analysis. *Viruses* 2, 1804–1820.
- Wu, L.Z., Sheng, Y.B., Xie, J. Bin, Wang, W., 2008. Photoexcitation of tryptophan groups induced reduction of disulfide bonds in hen egg white lysozyme. *J. Mol. Struct.* 882, 101–106.